



Calhoun: The NPS Institutional Archive

Theses and Dissertations

Thesis Collection

1974

Microwave interferometer measurements of electron removal in the argon afterglow

Adler, Robert E.

Monterey, California. Naval Postgraduate School

<http://hdl.handle.net/10945/17129>



Calhoun is a project of the Dudley Knox Library at NPS, furthering the precepts and goals of open government and government transparency. All information contained herein has been approved for release by the NPS Public Affairs Officer.

Dudley Knox Library / Naval Postgraduate School
411 Dyer Road / 1 University Circle
Monterey, California USA 93943

<http://www.nps.edu/library>

MICROWAVE INTERFEROMETER
MEASUREMENTS OF ELECTRON REMOVAL
IN THE ARGON AFTERGLOW

ROBERT E ADLER
AND
CLAUDE J. TETRICK

LIBRARY
U.S. NAVAL POSTGRADUATE SCHOOL
MONTEREY, CALIFORNIA

8854

ADLER

1959

MICROWAVE

THESIS
A25

ELECTRONIC

Letter on cover:

MICROWAVE INTERFEROMETER MEASURE-
MENTS OF ELECTRON REMOVAL IN THE
ARGON AFTERGLOW

ROBERT E. ADLER
AND
CLAUDE J. TETRICK

Claude J. Tetrick

MICROWAVE INTERFEROMETER MEASUREMENTS OF
ELECTRON REMOVAL IN THE ARGON AFTERGLOW

by

Robert E. Adler

//

Lieutenant, United States Navy

and

Claude J. Tetrick

Lieutenant, United States Navy

Submitted in partial fulfillment of
the requirements for the degree of

MASTER OF SCIENCE
IN
ELECTRICAL ENGINEERING

United States Naval Postgraduate School
Monterey, California

1 9 5 9

Thesis

H. S.

MICROWAVE INTERFEROMETER MEASUREMENTS OF
ELECTRON REMOVAL IN THE ARGON AFTERGLOW

by

Robert E. Adler

and

Claude J. Tetrick

This work is accepted as fulfilling
the thesis requirements for the degree of

MASTER OF SCIENCE

IN

ELECTRICAL ENGINEERING

from the

United States Naval Postgraduate School

ABSTRACT

Electron densities and collision frequencies in the late afterglow of argon gas discharges for pressures ranging from 0.334 mm Hg to 11 mm Hg were determined by a new experimental technique, which employs a microwave interferometer operated at X band frequencies.

Electron density and luminosity data obtained for argon indicate that recombination is dominant over this range of pressures. The pressure range investigated was characterized by a relatively low recombination coefficient.

The study was made at Lockheed Missiles and Space Division Research Laboratories at Palo Alto, California where the authors worked under the tutelage of Dr. Robert C. Gunton. They wish to express their sincere appreciation to Dr. Gunton and Mr. J. W. Christie of Lockheed and to Dr. A. E. Vivell of the United States Naval Postgraduate School at Monterey, California for advice and guidance in obtaining the results of this investigation.

TABLE OF CONTENTS

Section	Title	Page
1.	Introduction	1
2.	Theory	2
3.	The Microwave Interferometer	7
4.	The Discharge System	11
5.	Experimental Results	18
6.	Luminosity Studies	23
7.	Conclusions	29
8.	Bibliography	43

LIST OF ILLUSTRATIONS

Figure	Page
1. The Microwave Interferometer	8
2. Sample Photographs of Recorded Signals	9
3. The Discharge System	12
4. The Discharge Ringing Effect	13
5. Energy Absorption Versus Pressure	14
6. Illustration of the Ionization Mechanism	15
7. Horn Radiation Patterns	16
8. Reciprocal of Electron Density Versus Time	19-20
9. Collision Frequency Versus Pressure	21
10. Phototube Limiting Circuit	23
11. Luminosity Profiles	24-25
12. Reciprocal of \sqrt{I} Versus Time	27
13. Streak Pictures	28
14. Crystal Response Curves	39-40

TABLE OF SYMBOLS

Symbol	Units	Definition
B	weber/sq meter	Flux density
c	3×10^8 meter/sec	velocity of light
D	coulombs/meter ²	Electric Displacement
D _a	cm ² /sec	Ambipolar Diffusion Co-efficient
e	1.59×10^{-19} coulombs	charge of an electron
E	volts/meter	electric field strength
I	relative units	Luminosity Intensity
h	meters	height
H	ampere turns/meter	Magnetic Intensity
i	$\sqrt{-1}$	denotes imaginary number
J	amps/meter ²	current density
\bar{K}	1.38×10^{-23} watt-sec/degree Kelvin	Boltzmann constant
l	meters	distance
m	kilograms	mass of electron
N	electrons/cm ³	electron density
P	watts	power
p	mm. of Hg.	pressure
Q	cm ²	Collision cross-section
R	meters	radius
T _{ir}	degrees Kelvin	temperature
t	seconds	time: "l'sec" denotes 10 ⁻⁶ seconds
V	meter/sec	velocity
\propto	nepers/meter	attenuation
α_r	cm ³ /ion-sec	recombination coefficient

TABLE OF SYMBOLS

Symbol	Units	Definition
θ	rad/meter	phase constant; θ_0 is free space value
$\Delta\theta$	rad/meter	measured phase shift
ϵ_c	farads/meter	dielectric constant; ϵ_0 is free space value
Θ	radians or deg.	angle of phase shift
λ	meters	wavelength
λ	meters	characteristic diffusion length
ν	sec ⁻¹	electron-molecule collision frequency
τ	sec	electron decay time constant
γ	meter ⁻¹	propagation constant
ω	rad/sec	angular frequency
ω_p	rad/sec	plasma frequency
μ	henry/meter	permeability; μ_0 is the free space value
∇	length ⁻¹	gradient
z	length	direction of wave propagation

1. Introduction

With the advent of new experimental techniques, the complex phenomena of the removal of electrons from a gas discharge plasma has been the subject of renewed interest in gas discharges leading to numerous experimental investigations. The physicist, the communications engineer and the naval officer are all interested in these electron removal phenomena, for they are of practical importance in fields of missile communications [1,2,3] and in fusion research [4].

A new experimental technique using a microwave interferometer has been used here to determine electron-molecule collision frequencies and electron densities during the afterglow of an argon gas discharge. Similar techniques have been used by others in different frequency bands [5,6]. One author reports the use of a microwave interferometer to measure electron densities in the upper atmosphere [7].

Use of the microwave interferometer is advantageous in that a low power (non-disturbing) collimated microwave beam probes the plasma permitting high electron density measurements; and, because of the short wavelengths used, better resolution of spatial variations within a large plasma sample is permitted.

The interferometer method was used to determine the electron decay processes in pure argon gas at X band frequencies. Ionization of the gas was attained using a high voltage d-c discharge circuit.

The electron density spatial distribution and its variation with time were determined by mapping the luminosity of the discharge using a photomultiplier tube and delay circuit.

2. Theory

The methods of investigating gaseous discharges with microwave signals are based on the behavior of free electrons in an ionized gas under the influence of high frequency electromagnetic fields of low intensity.¹ For microwave signals-only the effects of electron behavior need be considered, because at very high frequencies the heavy positive ions oscillate a negligible amount and cannot contribute directly to the high frequency dielectric constant.

Assuming no external magnetic field, the propagation constant, γ , of an RF electromagnetic wave in an ionized gas is related to the complex dielectric constant², ϵ_c , by:

$$\gamma = j\omega\sqrt{\mu_0\epsilon_c}$$

$$\gamma = j\omega\sqrt{\mu_0\epsilon_0} \left[1 - \frac{\omega_p^2/\omega^2}{1 + \nu^2/\omega^2} - j \frac{\omega_p^2 \nu/\omega}{\omega^2(1 + \nu^2/\omega^2)} \right]^{\frac{1}{2}}$$

where ν is the electron-molecule collision frequency,

ω is the electromagnetic wave frequency and,

ω_p is the plasma frequency defined by

$$\omega_p = \left(\frac{Ne^2}{m\epsilon_0} \right)^{\frac{1}{2}}$$

The symbols m and e denote the mass and charge of an electron, N is the electron density in electrons per cubic meter and ϵ_0 is the free space dielectric constant. ($\frac{1}{36\pi \times 10^9}$ in mks units). Thus, values of

¹L. Goldstein [8] and Oskam [9] present comprehensive reviews of the microwave probing techniques in use and of significant results obtained using microwave methods.

²The exact theory of conductivity is given by Margenau [10].

electron density and collision frequency may be determined by measuring the real and imaginary parts of the propagation constant, defined as

$$\gamma = \alpha + i\beta$$

Equation (1) is derived in Appendix 1. The derivation assumes a Lorentzian gaseous medium wherein:

(a) the momentum transfer per electron-molecule collision is small and

(b) the change of motion of electrons can be ascribed to their collisions with only the molecules, the effect of mutual interaction between the light particles being negligible [9].

Further assumptions for the microwave probing technique employed are:

(c) the dimensions of the gas cell are significantly larger than both the amplitude of electron oscillations and the electron mean free path and,

(d) plane wave propagation of the microwaves through an unbounded plasma.

Two distinct regions of interest exist during the decay of a gaseous discharge. For the case $\omega_p > \omega$, which occurs immediately after excitation, the plasma acts like an ordinary ohmic conductor; an externally generated wave cannot propagate and is totally reflected at the boundary of the plasma. Then, when plasma frequency decreases below the microwave frequency the medium behaves as a low loss dielectric. Propagation resumes, but now the wave is attenuated and shifted in phase according to the plasma dielectric behavior.

Only the region wherein $\omega_p < \omega$ was investigated. Calculations for the variation of electron density with time in this region led to the determination of the dominant electron processes.

For low pressures³ electron density computations are often simplified by making the approximation to (1) for $\frac{\gamma^2}{\omega^2} \ll 1$ which implies that the angular frequency, ω , is sufficiently high so that no appreciable loss of electron energy occurs during a single cycle. Such is the case, for example, at great heights above the earth's surface. Similarly, during the late afterglow of a low pressure gas discharge this approximation may be made (See Appendix I).

ELECTRON LOSS PROCESSES

The basic electron removal processes [11] in the afterglow of a gas discharge are: volume recombination, ambipolar diffusion, and attachment to neutral molecules. Neglecting attachment, which does not occur in the noble gases, the basic electron loss processes may be described by:

$$\begin{aligned} \frac{\partial N}{\partial t} &= -\alpha_r N^2 + D_a \nabla^2 N \\ &= -\alpha_r N^2 - N \frac{D_a}{\lambda^2} \end{aligned} \quad (2)$$

where D_a is defined as the ambipolar diffusion coefficient and λ is the characteristic diffusion length associated with the lowest mode⁴ of diffusion. The solution of the equation yields

$$\frac{N}{1 + \alpha_r \tau N} = \frac{N_0}{1 + \alpha_r \tau N_0} \exp^{-t/\tau} \quad (3)$$

where τ is the time constant associated with the decay of electron density.

Values of α_r , the recombination coefficient, and D_a , the ambipolar diffusion coefficient, express the rate of removal of electrons by each of the two removal mechanisms. Equation (2) shows that electron removal by diffusion is in direct proportion to electron density, whereas removal by

³For argon the approximate equations could be used only for pressures less than 1 mm Hg.

⁴i.e. λ is the largest diffusion length associated with the longest decay time constant.

recombination is dependent upon the square of electron density.

It has been reported, for argon, that both ambipolar diffusion and recombination contribute significantly to the removal [12] of electrons in the 0.5-10 mm Hg range of gas pressures, depending on the method used in ionizing the gas. Below 0.5 mm ambipolar diffusion should dominate, and above 10 mm Hg electrons are removed primarily⁵ by recombination. When ambipolar diffusion is dominant, D_a may be obtained by first determining the time constant, τ , from a \log_{10} plot of electron density versus time: D_a is then computed as λ^2/τ where λ , the characteristic diffusion length [12] is defined by:

$$\frac{1}{\lambda^2} = \left(\frac{\pi}{h}\right)^2 + \left(\frac{2.4}{R}\right)^2$$

Above 10 mm Hg, α_r may be obtained, simply, as the slope of a plot of N^{-1} versus time.

For the pressure range wherein both mechanisms are comparable in magnitude the coefficients are more difficult to determine. The percentage contribution of the two processes to electron removal and the methods used to obtain the electron removal coefficients have frequently been discussed in the literature [9, 12]. One method of analysis is to assume the validity of the usually accepted value of $D_a \cdot p$, which is believed to be constant with pressure [8]. The effects of ambipolar diffusion may then be extracted from the electron decay rate and the recombination coefficient determined from (2).

⁵It should be realized that at all pressures, and more significantly at low pressures, the attachment to electronegative impurities will make some contribution to the electron removal process. Herein lies an important reason for using pure gases and obtaining low vacuum pressures before inserting a gas sample.

LUMINOSITY

During the decay period the plasma electron density distribution will rapidly tend to uniformity if the dominant electron loss mechanism is recombination. This results from the fact that the rate of electron loss is proportional to the square of electron density.

The light intensity, I , produced in the plasma by electron recombination is also proportional to the square of electron density. So, if recombination is the dominant loss process a plot of $1/\sqrt{I}$ versus time should be linear [12]. This assumes that there are no long-life metastables present, which is a valid assumption at higher pressures [13].⁶

The light distribution, following the end of discharge, was used as a qualitative measure of the spatial electron distribution of the decay period.

⁶Higher pressures are defined as being greater than 1 mm Hg.

3. The microwave interferometer

The arrangement of the microwave components into an interferometer is shown in Fig. 1. The microwave power source was an X band klystron operated CW. The power level of the klystron signal could be adjusted by means of attenuators in the test arm. Crystal detector mounts were used in conjunction with a Tektronix 531 oscilloscope using a high gain preamplifier to record transmitted, reflected and interferometer signal voltages versus time. Sample photographs of these signals are shown in Fig. 2.

The interferometer bridge was adjusted using the phase shifter in the reference path to obtain a 180° phase difference between the reference and test signals. Thus, when $N = 0$, $\beta = \beta_0$, the free space phase shift per unit length. The reference attenuator was then adjusted to obtain a null indication at the interferometer crystal.

Average power of the microwave signal incident on the plasma was measured as 0.2 milliwatts using a power meter and thermistor mount.

Photographs of the interferometer and transmitted signals were used to obtain phase change, $\Delta \beta$, of microwave signals passing through the plasma.⁷ This phase change is attributed to the real part of the plasma dielectric constant, which is a function of the electron density, N , and ν , the electron-molecule collision frequency. The attenuation, \propto , of the electromagnetic wave propagating through the decaying plasma is attributed to electron collisions with neutral molecules. This value was determined from the incident, transmitted and reflected signals.

All results were obtained at a frequency of 8760 mcs. This frequency

⁷Errors in the interferometer signal which, conceivably, might result due to reflections off the plasma were found to be negligible for the case $\omega_p < \omega$ [6].

THE MICROWAVE INTERFEROMETER

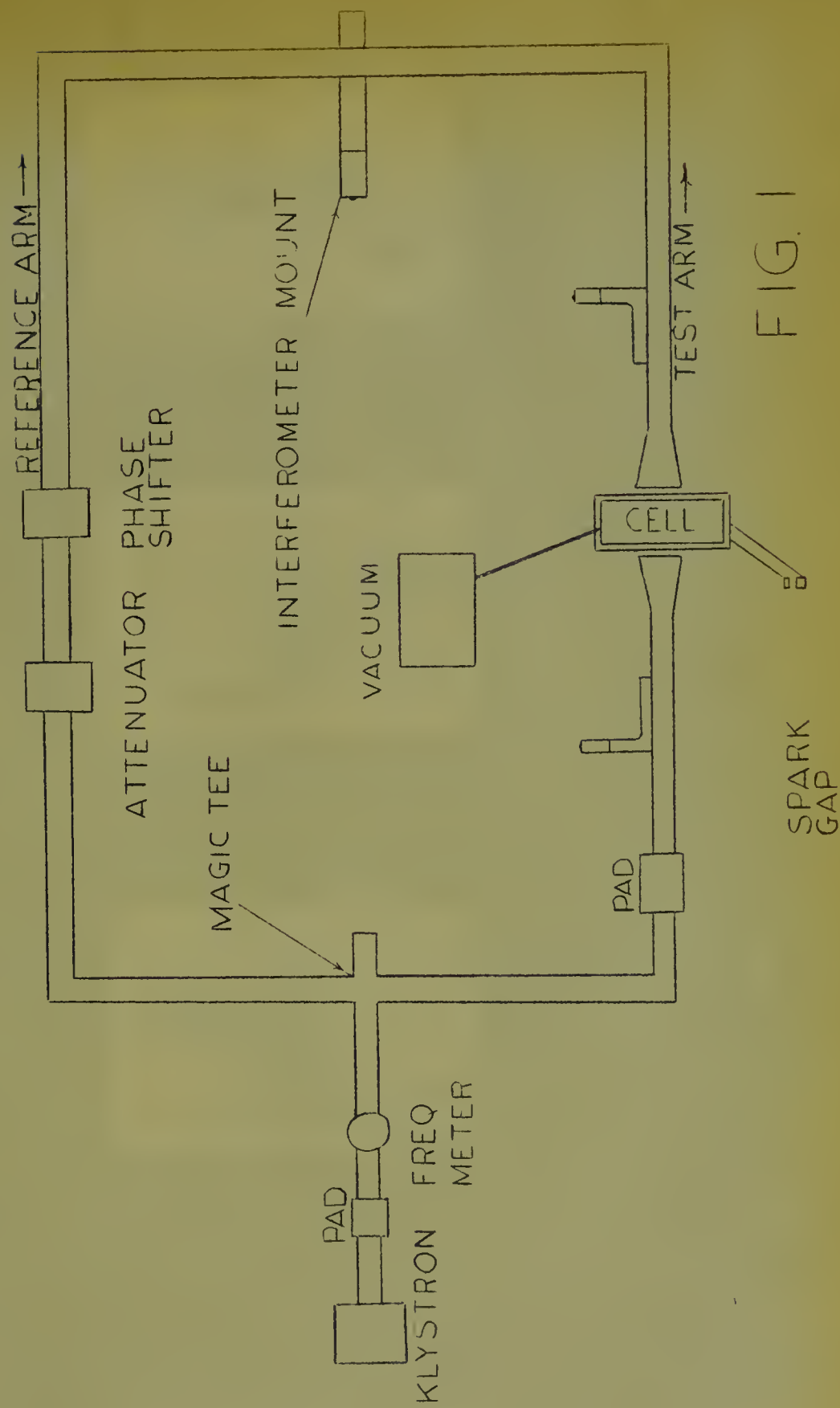
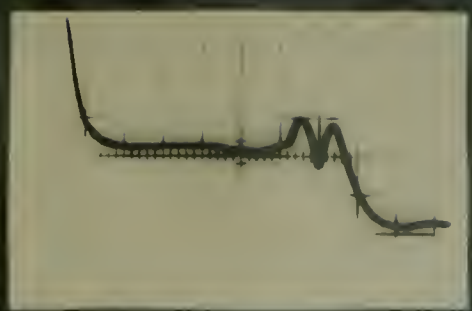
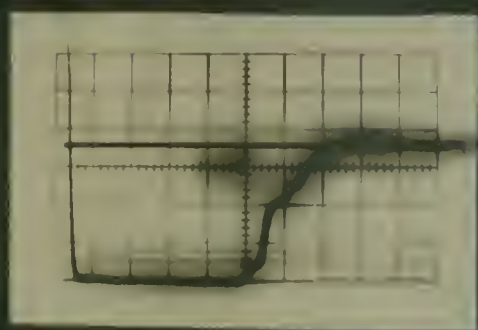


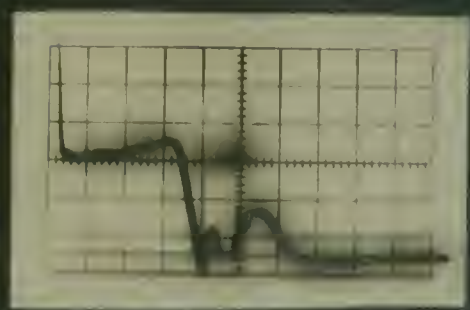
FIG. 1



P. OVERCOMPT



P. OVERCOMPT



P. OVERCOMPT

FIG. 2; TABLE 1, 2, 3, 4, 5, 6, 7, 8, 9, 10, 11, 12, 13, 14, 15, 16, 17, 18, 19, 20, 21, 22, 23, 24, 25, 26, 27, 28, 29, 30, 31, 32, 33, 34, 35, 36, 37, 38, 39, 40, 41, 42, 43, 44, 45, 46, 47, 48, 49, 50, 51, 52, 53, 54, 55, 56, 57, 58, 59, 60, 61, 62, 63, 64, 65, 66, 67, 68, 69, 70, 71, 72, 73, 74, 75, 76, 77, 78, 79, 80, 81, 82, 83, 84, 85, 86, 87, 88, 89, 90, 91, 92, 93, 94, 95, 96, 97, 98, 99, 100

was used to give the best impedance match for the pyrex cell. The wall thickness of the pyrex cell acted as a quarter wave plate at this frequency- thus, reflection from the cell was minimized.

4. The discharge system

A simplified diagram of the discharge system is shown in Fig. 3. The discharge cylinder consisted of a 10.5 cm diameter pyrex cell, 5 cm wide, with a copper strap encircling the entire circumference of the cell. The high vacuum system was constructed of glass and used a 3-stage oil fractionating diffusion pump. The vacuum pump was equipped with a liquid nitrogen trap made of metal. A vacuum of 8×10^{-7} mm Hg, measured with an ion gauge, was maintained by the system. The vacuum system was heated and outgassed after each series of data. Cell gas pressures were measured by a manometer filled with Octoil S diffusion pump oil, which has a vapor pressure of 10^{-8} mm Hg at room temperature. Air Reduction Sales spectroscopically pure argon was used for all measurements.

Energy was stored at 28 kv in a 1.1 uf low inductance capacitor. A thyratron excited spark gap discharged the capacitor through the copper strap. The discharge oscillated at 3.6×10^5 cycles per second and was damped to zero in 20 usec. Sample photographs of this effect are shown in Fig. 4.

Comparison of the damping time constant for the evacuated cell with damping time constants for various cell gas pressures provided a measure of energy dissipation in the gas, since the change in time constant was a measure of plasma resistivity. The variation of the energy absorbed by the gas for various gas pressures is illustrated in Fig. 5. It should be noted that at very low gas pressures the gas absorbed very little energy. This is attributed to the large mean free path of electrons, hence low electron-molecule collision frequencies.

The mechanism of gas ionization may best be described by considering Fig. 6.

THE DISCHARGE SYSTEM

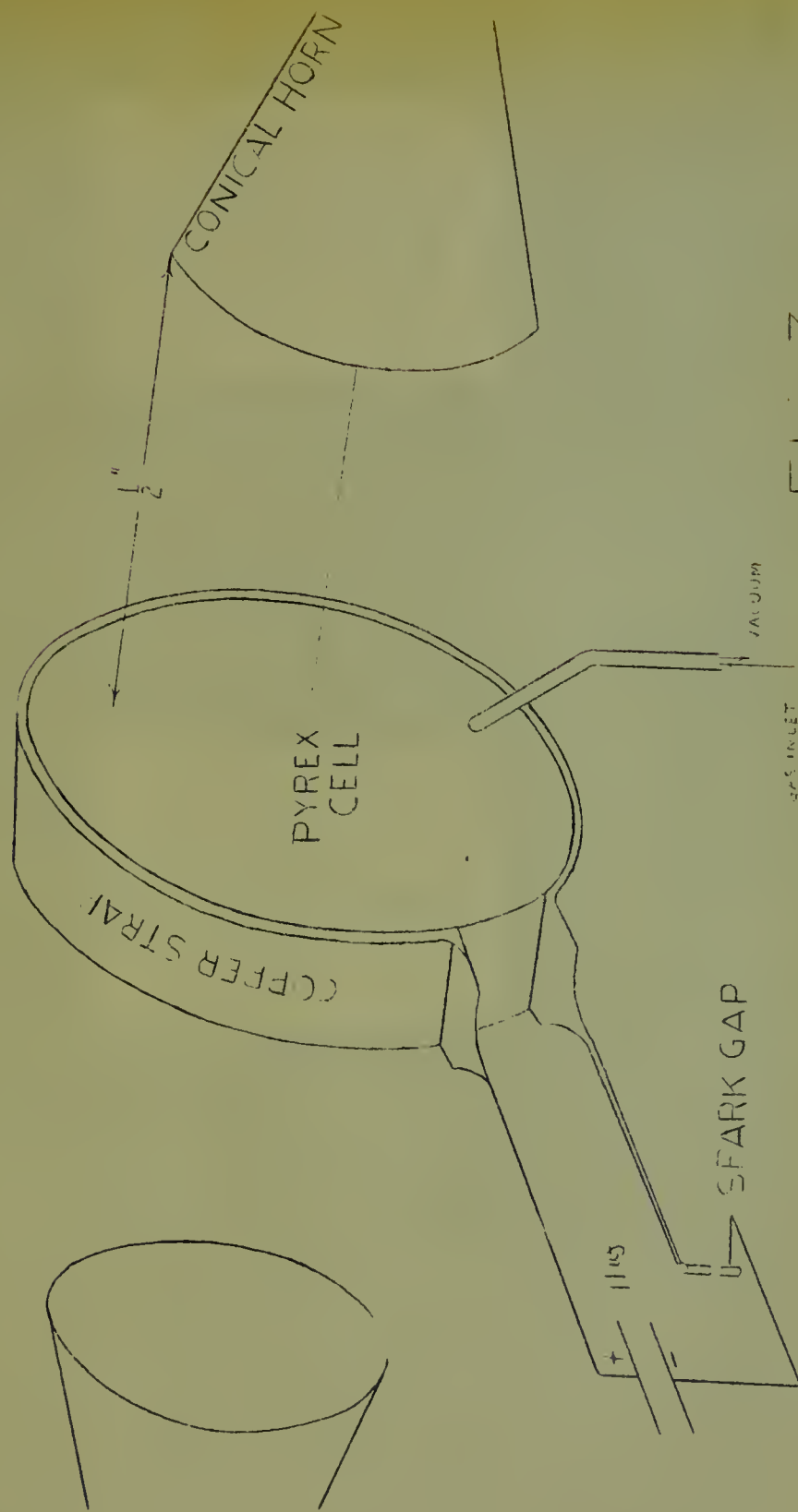
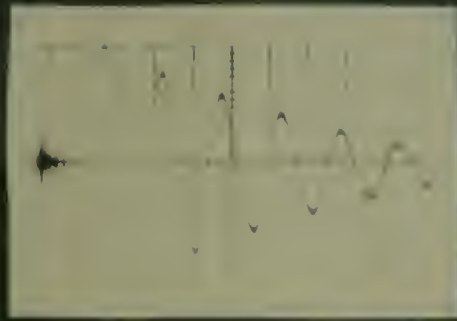
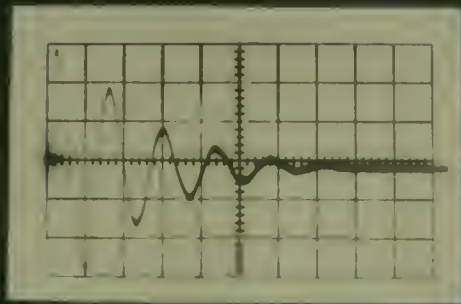


FIG. 3



CHARGING EFFECT FOR LYCATEL CELL

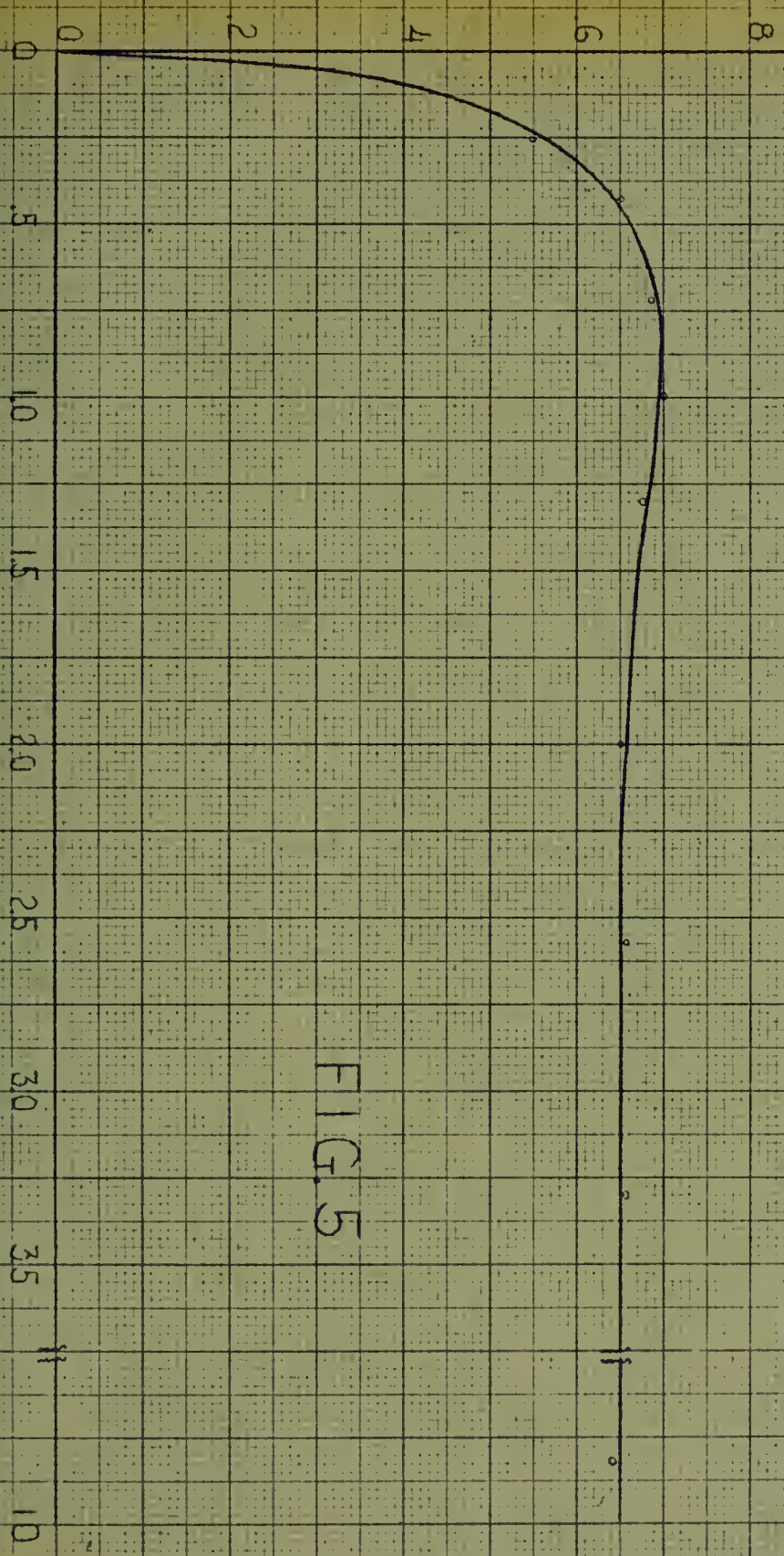


CHARGING EFFECT FOR 0.6 MEG CELL HAS BEEN

FIG. 4; THE DISCHARGE CHARGING EFFECT

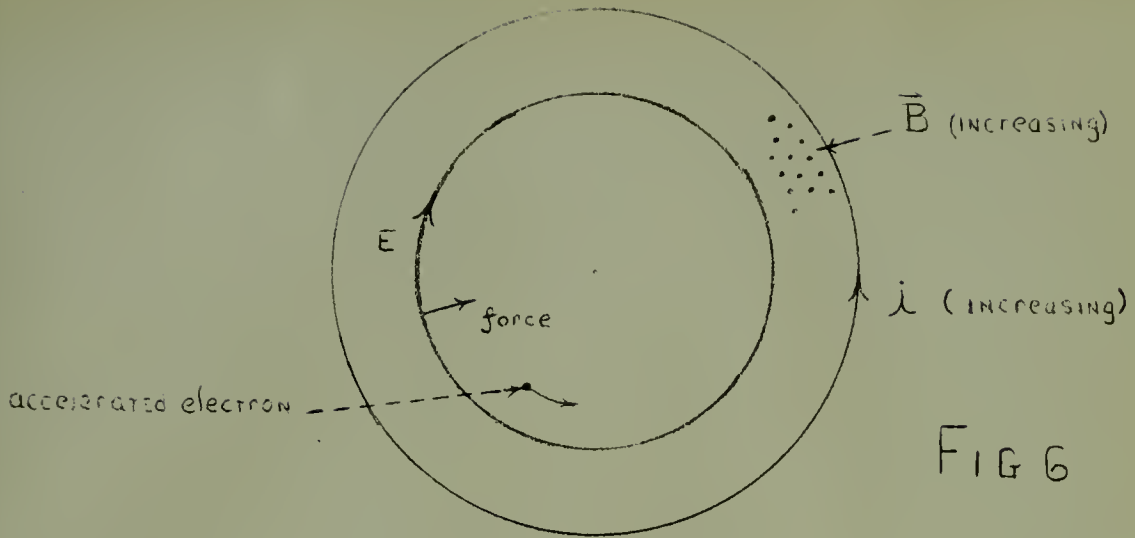
ENERGY ABSORPTION VS PRESSURE

ENERGY ABSORBED BY GAS-ARBITRARY UNITS



$E_{\text{PRIMARY}} = 28.5 \text{ KV}$

FIG. 5



The coupling of energy stored in the capacitor to the gas in the cell is analogous to transformer coupling. Strap discharge current creates a magnetic field according to Maxwell's equation

$$\nabla \times H = I$$

neglecting the displacement current term. An electric field is introduced by the changing magnetic field according to

$$\nabla \times E = - \frac{\partial B}{\partial t}$$

This field produces high energy collisions of residual electrons with the gas molecules - producing electrons and ions. A current opposite to the direction of strap current flows producing an inward force that serves to further ionize the gas.

Conical horns were located at the center of the circular cell face. The far field radiation patterns of the horns were measured and the results illustrated in Fig. 7. Commercial high gain pyramidal horns did not give

HORN RADIATION PATTERN

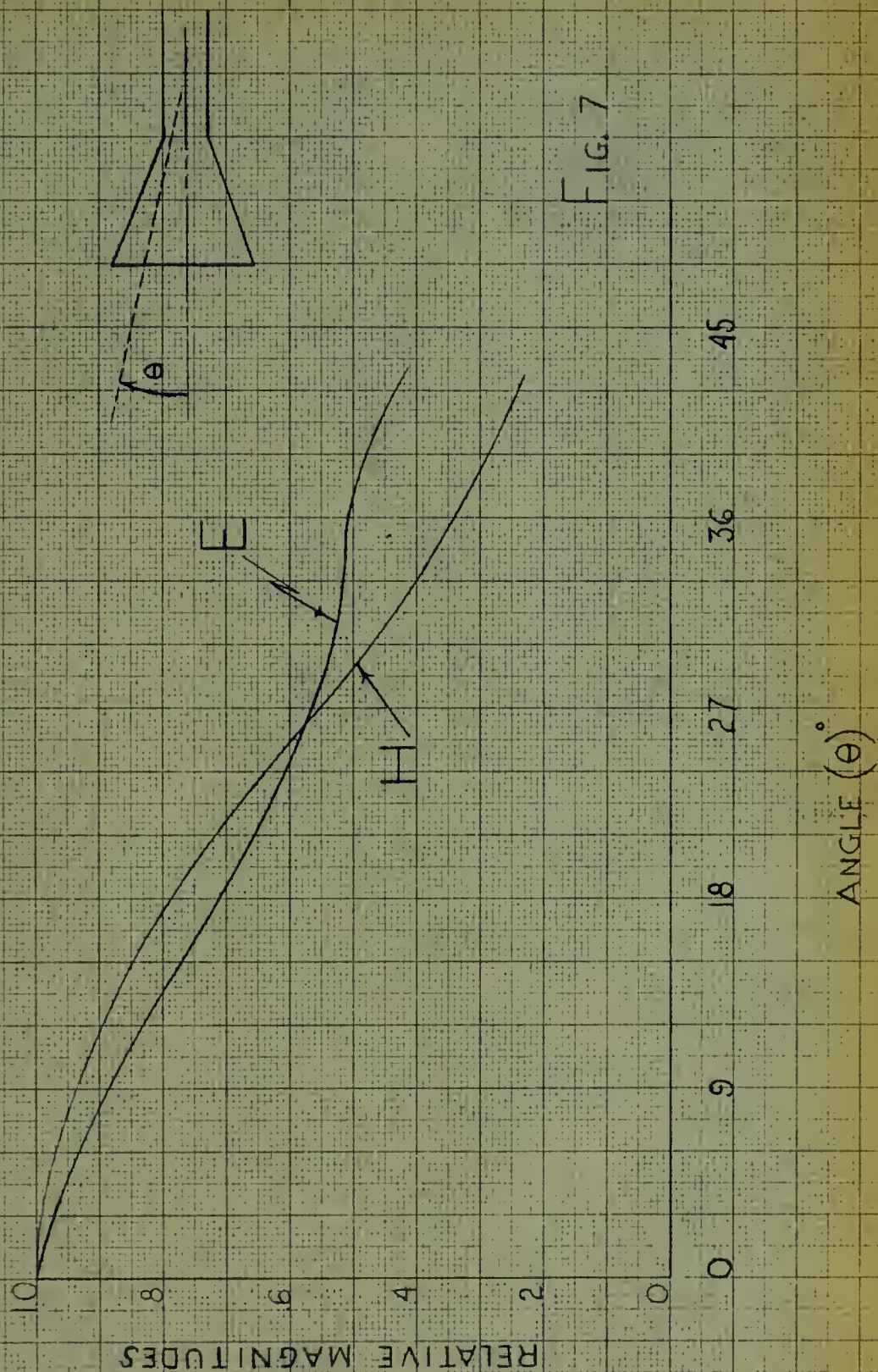


FIG. 7

smooth E and H field radiation patterns such as were exhibited by the conical horns [15].

The oscilloscope used to measure transmitted, reflected and interferometer signals was triggered by an RCA 931-A photomultiplier tube which "looked" at the light emitted by the discharge. The phototube was connected to a variable delay circuit which, in turn, started the oscilloscope sweep. This arrangement permitted observation of any region of the discharge on an expanded time base.

5. Experimental results

Sample photographs of signals obtained for argon are shown in Fig. 2. Formulas (11) and (12)⁸ of Appendix I were applied to data interpreted from signals such as these to obtain electron densities and collision frequencies for five gas pressures. Only those portions of the signals after transmission had resumed (ie $\omega_p < \omega$) were analyzed. This region is most obvious in the transmitted signal, where, after a lengthy cut-off period the signal returns slowly to the original transmitted level. A sample calculation is made in Appendix II.

In order to determine the dominant electron removal processes- values of N^{-1} and $\log_{10} N$ were plotted versus time for each pressure. Ambipolar diffusion was found to be a negligible electron removal process ($< 2\%$) throughout the pressure range, so only the N^{-1} versus time plot has been presented (Fig. 8). However, to ensure the accurate determination of recombination coefficient- the small effects of ambipolar diffusion were extracted from the electron density results in a trial calculation using Redfield and Holts' value of $D_a \cdot p = 150$ [11]. Values of α_r obtained by this procedure varied very little from values obtained, simply, as the slope of the N^{-1} lines of Fig. 8. The largest value obtained for the recombination coefficient was $2 \times 10^{-8} \text{ cm}^3/\text{ion-sec}$. This calculation is made in Appendix II.

Fig. 9 illustrates the variation of average electron-molecule collision frequencies with pressure.

To ensure the reproducibility of the results obtained-two experimental conditions were varied: (1) the excitation voltage was varied

⁸When $(\frac{v}{\omega})^2 \ll 0.01$ formulas (15) and (16) were used to obtain electron densities and collision frequencies. These are the approximation formulas, which considerably simplify the computations.

N^{-1} vs TIME

FIG. 8(a)

TIME AFTER DISCHARGE (min)

9.5

9.0

8.5

8.0

7.5

$N \times 10^{11}$

$\text{cm}^{-2}/10^4$

$P = 11 \text{ mm.}$

$P = 4.5 \text{ mm.}$

$P = 6.23 \text{ mm.}$

N^{-1} vs TIME

$N (X 10^{-11}) \text{ cm}^3 / \text{ION}$

TIME AFTER DISCHARGE (milli sec)

1.00 1.05 1.10 1.15 1.20 1.25 2.57 2.62 2.67 2.72 2.77 2.82

$P = 334 \text{ mm}$

$P = 121 \text{ mm}$

Fig. 8 (a)

COLLISION FREQUENCY VS PRESSURE

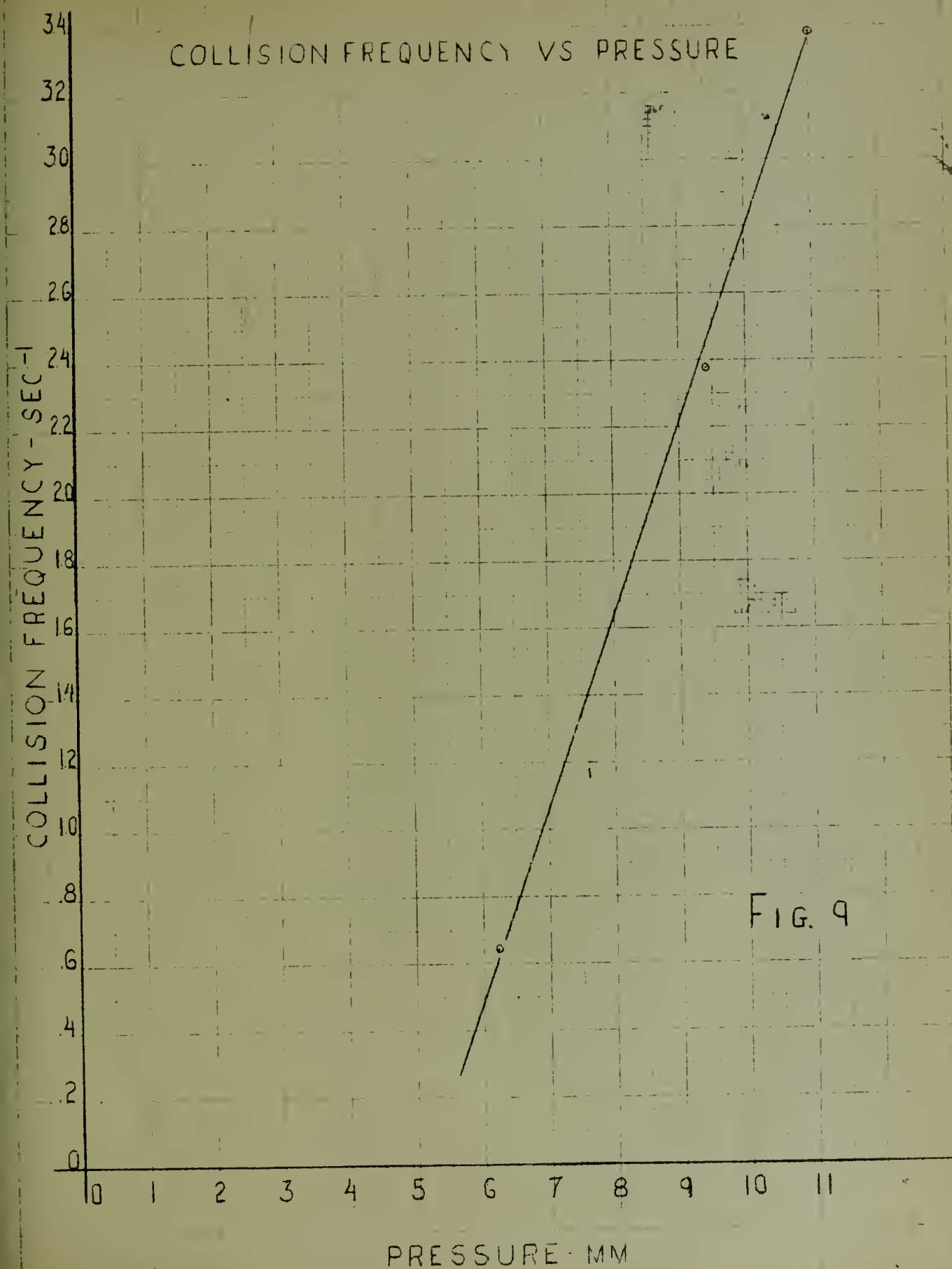


FIG. 9

from 22 kv to 20 kv, and 2 the conical horns were placed at various distances from the pyrex cell. No significant change in data occurred for these variations.

6. Luminosity studies

The luminous glow of the discharge was observed in order to determine the electron distribution within the cell and to determine whether or not recombination was dominant.

A shielded 931-A photomultiplier tube was moved along the diameter and along the edge of the cell. The photomultiplier was connected to a Tektronics 531 oscilloscope through a diode limiting circuit. The limiting circuit was necessary to prevent the large initial output voltage of the photomultiplier from being applied to the scope input capacitor. This circuit is shown in Fig. 10.

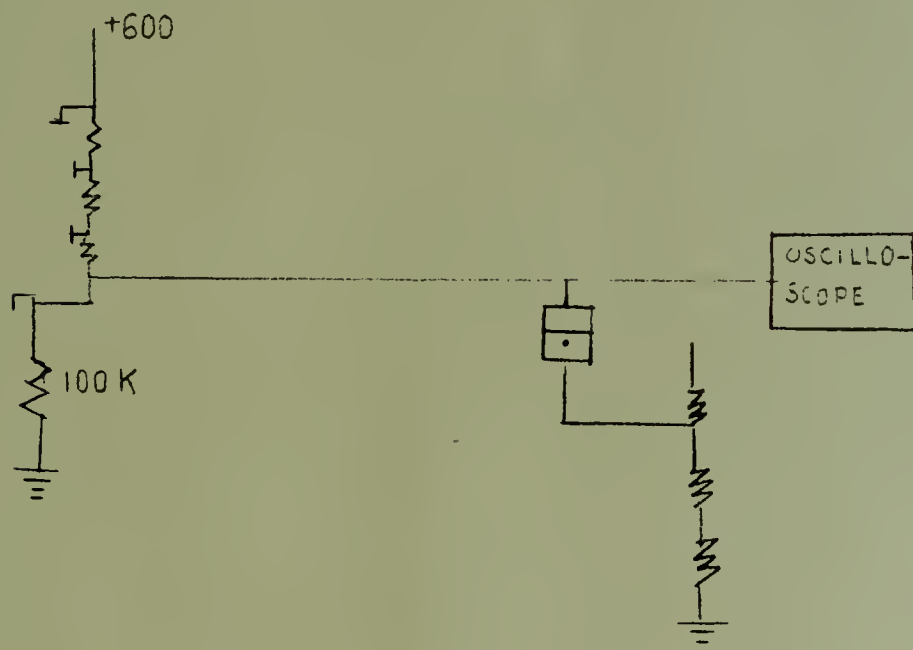
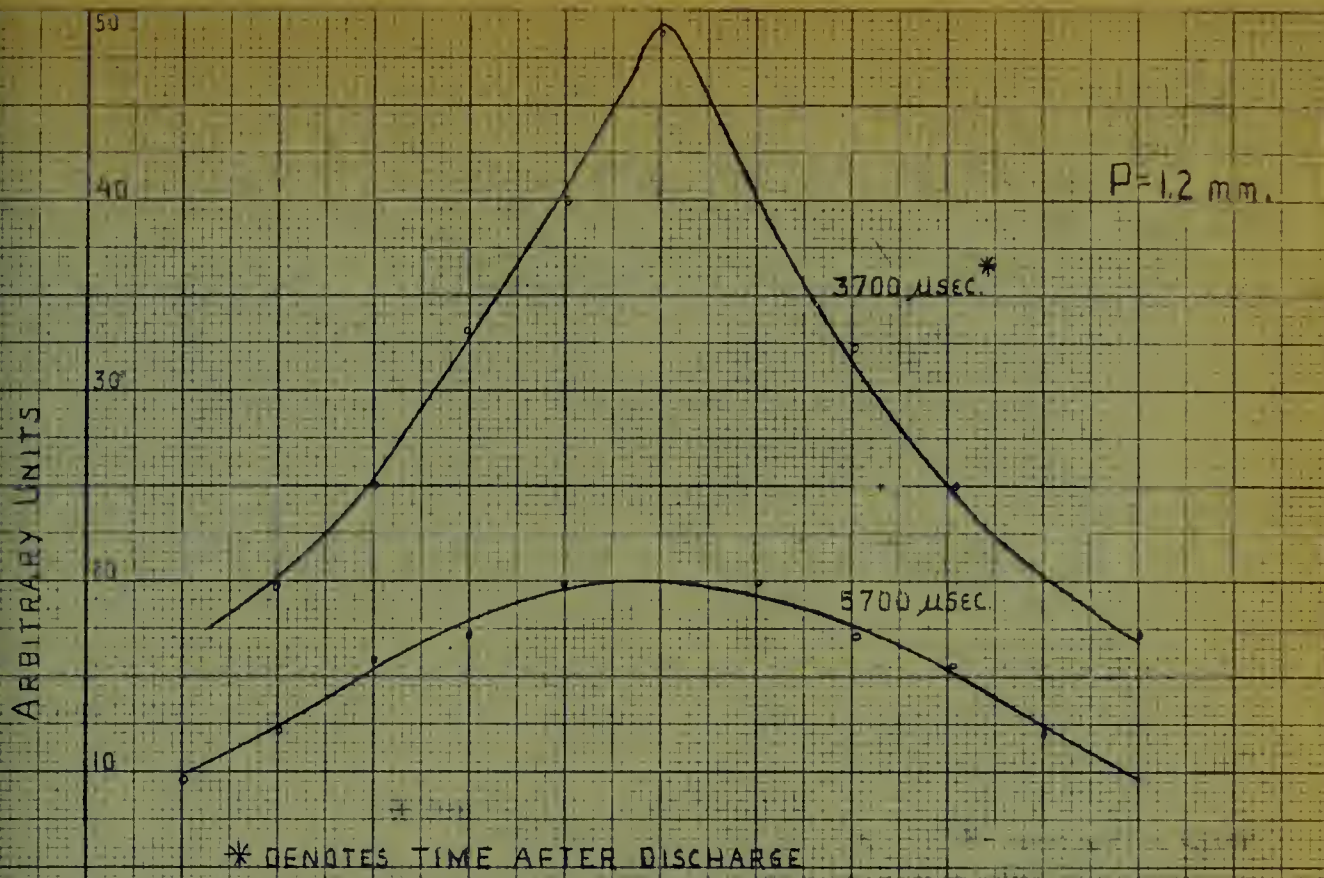
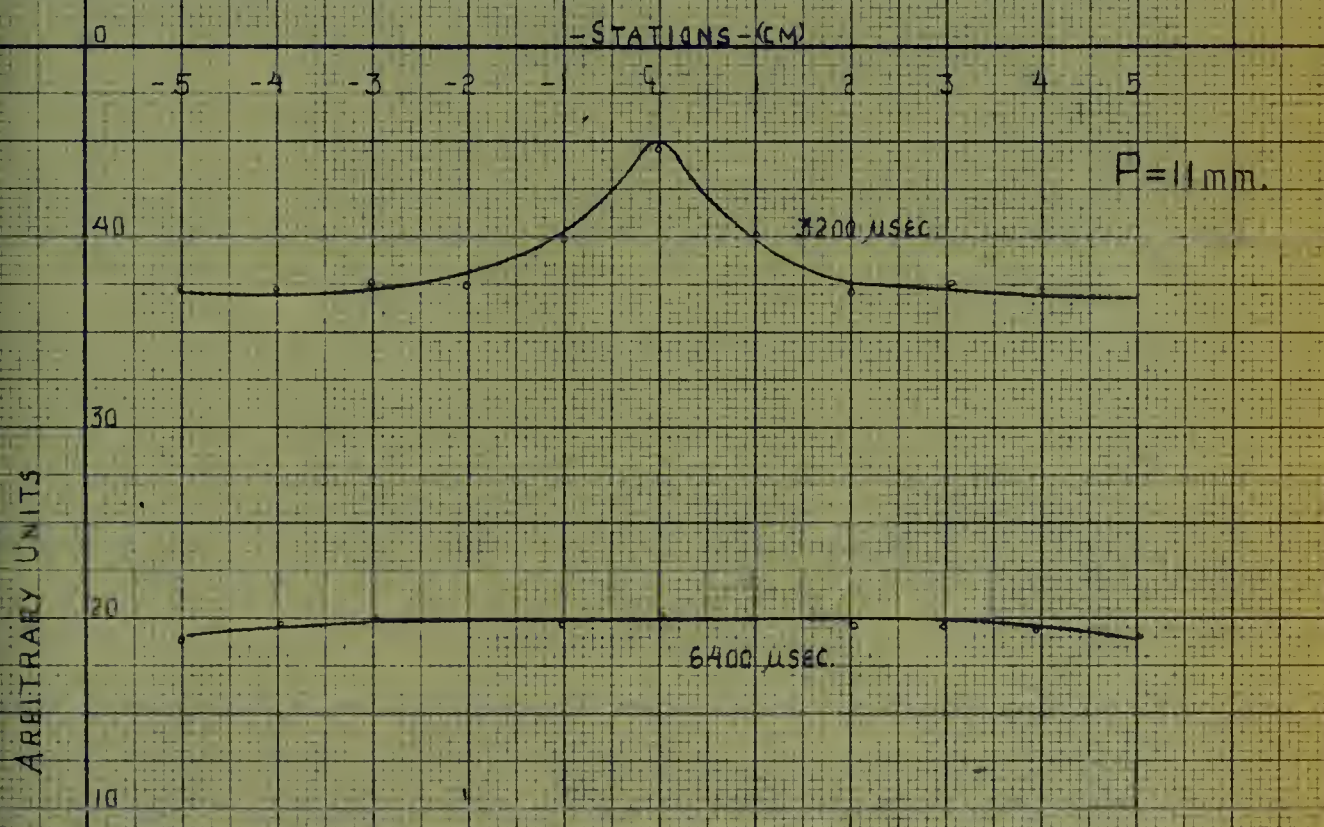


Fig. 10

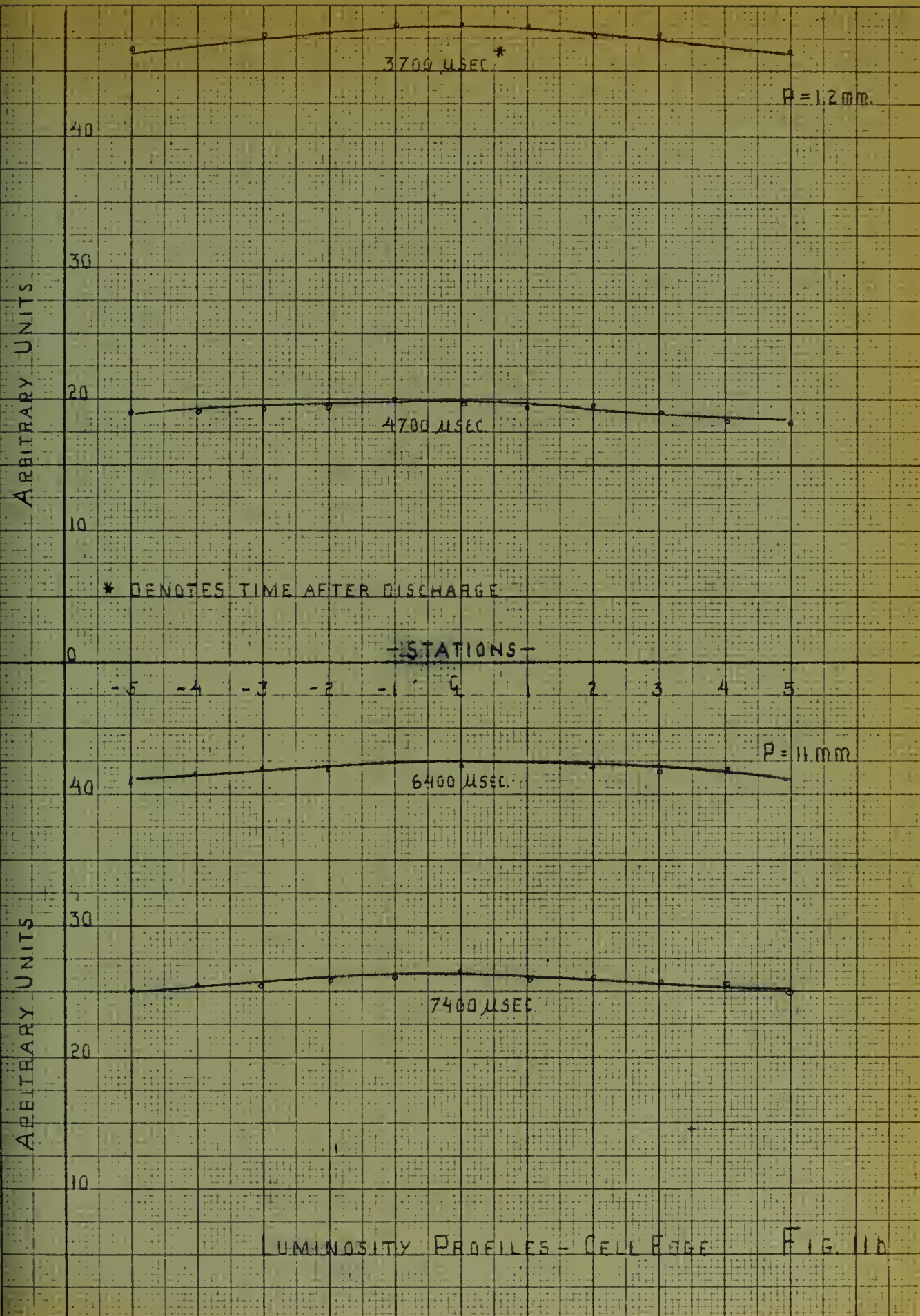
The oscilloscope reproduced the light intensity of the plasma normal to the cell wall for each station. The oscilloscope was triggered by another photomultiplier operated through a variable delay circuit in order to observe the light distribution over the same period of time for which electron density measurements were taken. Figs. 11a and 11b illustrate the intensity distributions obtained for the extremes of the pressure range investigated. The electron distribution at high pressures appeared to be trape-



* DENOTES TIME AFTER DISCHARGE



LUMINOSITY PROFILES-CELL DIAMETER FIG. 11a



zoidal, and at low pressures the distribution was triangular.

A plot of $1/\sqrt{I}$ versus time is shown in Fig. 12. It compares favorably with the reciprocal of electron density. The linearity of the $1/\sqrt{I}$ plot suggests that recombination is dominant.

An image converter streak camera was used to take photographs across the diameter of the cell. The cell was covered with black tape except for a 1/8" slit along a diameter and pictures were taken for various gas pressures to observe the electron distribution in the cell after discharge. The pictures (Fig. 13) indicate that strong gas discharges create shock waves along the cell edges, which are regions of high electron density [16]. As the cell pressure is decreased the shock waves form nearer the cell center. In all cases the high concentrations of electrons at the edge of the cell is rapidly dissipated by the end of 200 usec.

\sqrt{I} VS TIME

11.5

5

10

9

8

7

6

5

4

3

2

1

0

ARBITRARY UNITS

$N_+ (\times 10^{-10})$

$P = 9.45 \text{ MM}$

$a - N^{-1}$

$b - I^{-1/2}$

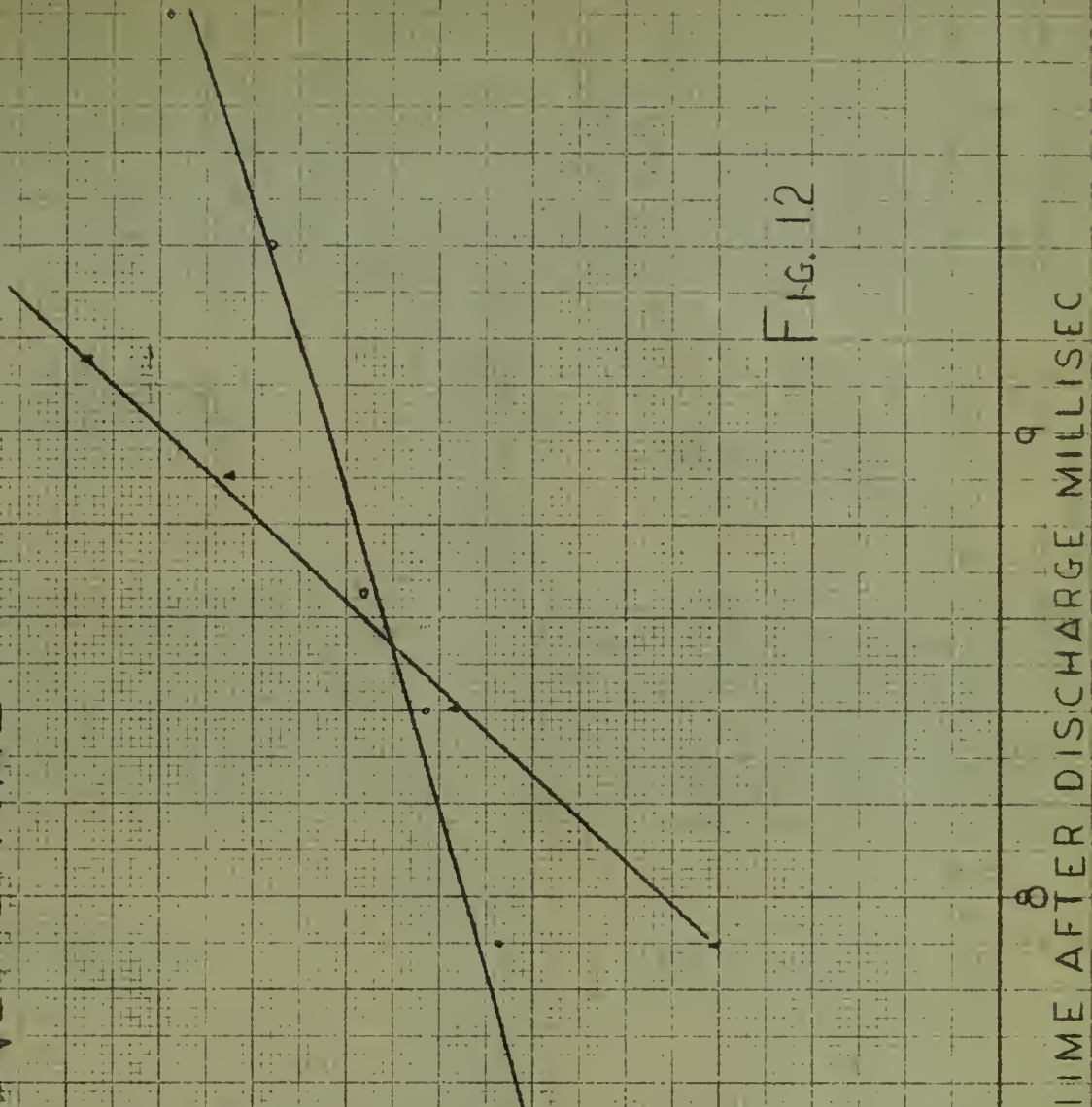
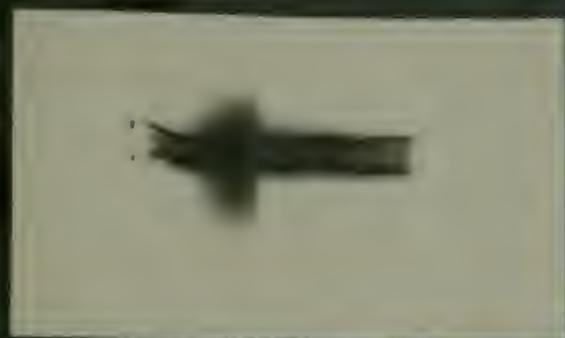


FIG. 12

TIME AFTER DISCHARGE MILLISEC

11.1 = 11.1 A. HG.

11.2 = 11.2 A. HG.



10 UNC A. HG.



13.2 UNC A. HG.

13.1; 13.2 A. HG.

7. Conclusions

For the pressures studied it was determined by electron density calculations that the dominant electron loss process was recombination. This was confirmed by luminosity studies. For 0.334 mm Hg and 1.21 mm Hg the recombination coefficient was, approximately, $2 \times 10^{-8} \text{ cm}^3/\text{ion-sec}$, whereas, for the three higher pressures, values were all close to $4 \times 10^{-9} \text{ cm}^3/\text{ion-sec}$. The higher values of α_p at lower pressures could, possibly, be attributed to non-uniform electron density distributions at the time measurements were taken (See Fig. 10). The triangular density distribution indicates higher recombination rates at the cell center.

The contribution of ambipolar diffusion to the removal of electrons in the afterglow was unexpectedly low. This occurred primarily because recombination varied as N^2 and ambipolar diffusion depended only on N . So, for the high electron densities measured, recombination was dominant.

Very little comparison of results with other findings can be made since the electron densities studied were of the order of 10^2 higher than what has previously been reported. Redfield and Holt [12] obtained an approximate value of $4 \times 10^{-8} \text{ cm}^3/\text{ion-sec}$ for α_p in the same pressure range, but computations were made for lower electron densities, where ambipolar diffusion was found to be a significant electron removal mechanism.

The values of electron-molecule collision frequency were found to be larger than those predicted by kinetic theory [17].

No spectroscopic studies were made of the gas discharge, but it is believed that recombination was measured for the A_2^+ ion instead of the short-lived A^+ ion [18, 19].

APPENDIX I

General equations yielding $(\frac{\gamma}{\omega})^2$ and $(\frac{\omega_p}{\omega})^2$ may be derived in terms of the attenuation factor, α , and phase shift constant, β , both of which may be determined by microwave interferometer measurements. The approximation for $(\frac{\gamma}{\omega})^2 \ll 1$ may then be made to simplify calculations for electron-molecule collision frequency and electron density in the late afterglow of the discharge period.

Maxwell's equations are used in deriving the one-dimensional wave equation which may be expressed as:

$$\nabla^2 E - \gamma^2 E = 0 \quad (1A)$$

A solution to (1A) is:

$$E = E_0 \exp^{i\omega t - \gamma z} \quad (2A)$$

where wave propagation is in the "z" direction, which is parallel to the longitudinal axis of the waveguide.

In (1A):

$$\gamma, \text{ the propagation constant} = \alpha + i\beta = i\omega \sqrt{\mu \epsilon_c}$$

$$\beta, \text{ the phase shift/length} = \frac{2\pi}{\lambda} = \omega \sqrt{\mu \epsilon_c}$$

(denote free space value as β_0)

and attenuation factor = α

The complex dielectric constant in (1A), ϵ_c , is derived [20] from Maxwell's equation relating the curl of magnetic field to current:

$$\nabla \times \vec{H} = \vec{\dot{D}} + \vec{J} = i\omega \epsilon_c \vec{E} + Ne \vec{v} \quad (3A)$$

and

$$\vec{E} e = m \frac{d\vec{v}}{dt} + m \vec{v} \cdot \vec{v} \quad (4A)$$

which is the simple equation of motion for an electron in an electric field. Here $\vec{E} = E_0 \cos \omega t$ and \vec{v} is the velocity of an electron.

A solution for (4A) is

$$\vec{v} = \frac{\vec{E} e}{m \vec{v} + \lambda \omega m}$$

Equations (3A) and (4A) are solved then for the curl of the magnetic field yielding:

$$\nabla \times \vec{H} = \lambda \omega \vec{E} \epsilon_c \quad (5A)$$

where:

$$\epsilon_c = \epsilon_0 \left[1 - \frac{\omega_p^2}{\omega^2 (1 + \frac{v^2}{\omega^2})} - j \frac{\omega_p^2 \frac{v}{\omega}}{\omega^2 (1 + \frac{v^2}{\omega^2})} \right] \quad (6A)$$

and

$$\omega_p = \left(\frac{N e^2}{m \epsilon_0} \right)^{\frac{1}{2}}$$

To simplify the derivation of $\frac{v^2}{\omega^2}$ and $\frac{\omega_p^2}{\omega^2}$ let

$$K = 1 - \frac{\omega_p^2 / \omega^2}{1 + v^2 / \omega^2}$$

Then (6A) becomes

$$\epsilon_c = \epsilon_0 \left[K - j(1-K) \frac{\gamma}{\omega} \right] \quad (7A)$$

and the propagation constant is now

$$\gamma = \alpha + j\beta = j\omega \sqrt{\mu_0 \epsilon_0} \left[K - j(1-K) \frac{\gamma}{\omega} \right]^{\frac{1}{2}} \quad (8A)$$

The attenuation and phase shift factors may then be written as:

$$\alpha = \text{Imag.} \left[K - j(1-K) \frac{\gamma}{\omega} \right]^{\frac{1}{2}} (-\beta_0)$$

$$\alpha = -\beta_0 \sqrt{K} \sqrt{\frac{-1 + \sqrt{1 + \frac{(1-K)^2 (\frac{\gamma}{\omega})^2}{K^2}}}{2}} \quad (9A)$$

$$\beta = -\beta_0 \text{Re} \left[K - j(1-K) \frac{\gamma}{\omega} \right]^{\frac{1}{2}}$$

$$\beta = \beta_0 \sqrt{K} \sqrt{\frac{1 + \sqrt{1 + \frac{(1-K)^2 (\frac{\gamma}{\omega})^2}{K^2}}}{2}} \quad (10A)$$

Solving (9A) and (10A) for k in terms of α and β :

$$K = \frac{\beta^2 - \alpha^2}{\beta_0^2} \quad (11A)$$

Substituting K in (10A) then:

$$\left(\frac{\gamma}{\omega} \right)^2 = \frac{\left(\frac{\beta^2 + \alpha^2}{\beta_0^2} \right)^2 - \left(\frac{\beta^2 - \alpha^2}{\beta_0^2} \right)^2}{\left(1 - \frac{\beta^2 - \alpha^2}{\beta_0^2} \right)^2} \quad (12A)$$

Also, from (11A) and the expression relating K to ω_p , the plasma frequency:

$$\left(\frac{\omega_p}{\omega}\right)^2 = \left(1 - \frac{\beta^2 - \alpha^2}{\beta_0^2}\right) \left(1 + \frac{\gamma^2}{\omega^2}\right) \quad (13A)$$

The left sides of equations (12A) and (13A) represent the quantities which may be calculated using measured values of attenuation and phase shift of high frequency signals through a plasma assuming plane wave propagation.

For $\frac{\gamma^2}{\omega^2} \ll 1$, which is discussed on page⁹ four.

$$\frac{\alpha}{\omega} \approx \frac{\omega_p^2 / \omega^2 \left(\frac{\gamma}{\omega}\right)}{\left[1 - \frac{\omega_p^2}{\omega^2}\right]^{\frac{1}{2}}} \left(\frac{1}{2c}\right) \quad (14A)$$

$$\frac{\beta}{\omega} \approx \frac{1}{c} \left[1 - \frac{\omega_p^2}{\omega^2}\right]^{\frac{1}{2}} \quad (15A)$$

Substituting

$$\beta = \beta_0 - \Delta\beta$$

where $\Delta\beta$ represents the measured phase shift:

$$\gamma = c \frac{\left[1 - \frac{c}{\omega} \Delta\beta\right] \alpha}{1 - \left(1 - \frac{c}{\omega} \Delta\beta\right)^2} \quad (16A)$$

⁹A trial calculation should be made to ensure that the assumption is warranted.

$$N = \frac{m \epsilon_0}{e} \left[2 \Delta \beta \omega c - \Delta \beta^2 c \right] \quad (17A)$$

Note: It should be noted that the theory developed above is for the special case of the exact theory of Margenau [10]. This is the case of "constant collision frequency" for which

$$\gamma = \rho Q v$$

$$\text{and } Q v = \text{constant} \quad [21]$$

$$Q \propto \frac{1}{v}$$

This is strictly true only for the "Maxwellian" model of the molecule in which the molecule repels the colliding electron with a force in proportion to the inverse fifth power of the distance [9].

Actual gases depart from this behavior to some extent, having different $Q (v)$ relationships. However, these typically alter the results by a small factor and are not considered here.

Also, the theory above is a "weak field" theory, assuming that the probing microwave power is too small to alter, significantly, the temperature of the electrons.[9].

APPENDIX II

SAMPLE CALCULATION

A sample calculation using data obtained for a cell gas pressure of 0.45 mm Hg. at 8900 usec after discharge is made. Results of all calculations are condensed in the attached table.

Voltages were read from the interferometer, transmitted and reflected signal photographs for the specified time. These values were then converted to power readings using the crystal response curves (Fig. 14). Reference levels for each signal were obtained by shorting the transmitting horn and obtaining reference voltages, thence reference powers. All powers were normalized to the reference level power:

$$P'_{INT} = \frac{P_{INT}}{P_{REF}} = \frac{.68}{2.7} \times 100 = 25.2$$

$$P'_{TRAN} = \frac{P_{TRANS}}{P_{REF}} = \frac{13}{24.5} \times 100 = 53.0$$

$$P'_{REFL} = \frac{P_{REFL}}{P_{REF}} = \frac{2.66}{26.8} \times 100 = 9.95$$

$$\cos \theta = \frac{100 + P'_{TRAN} - P'_{INT}}{20 \sqrt{P'_{TRAN}}} = .878 \quad (22)$$

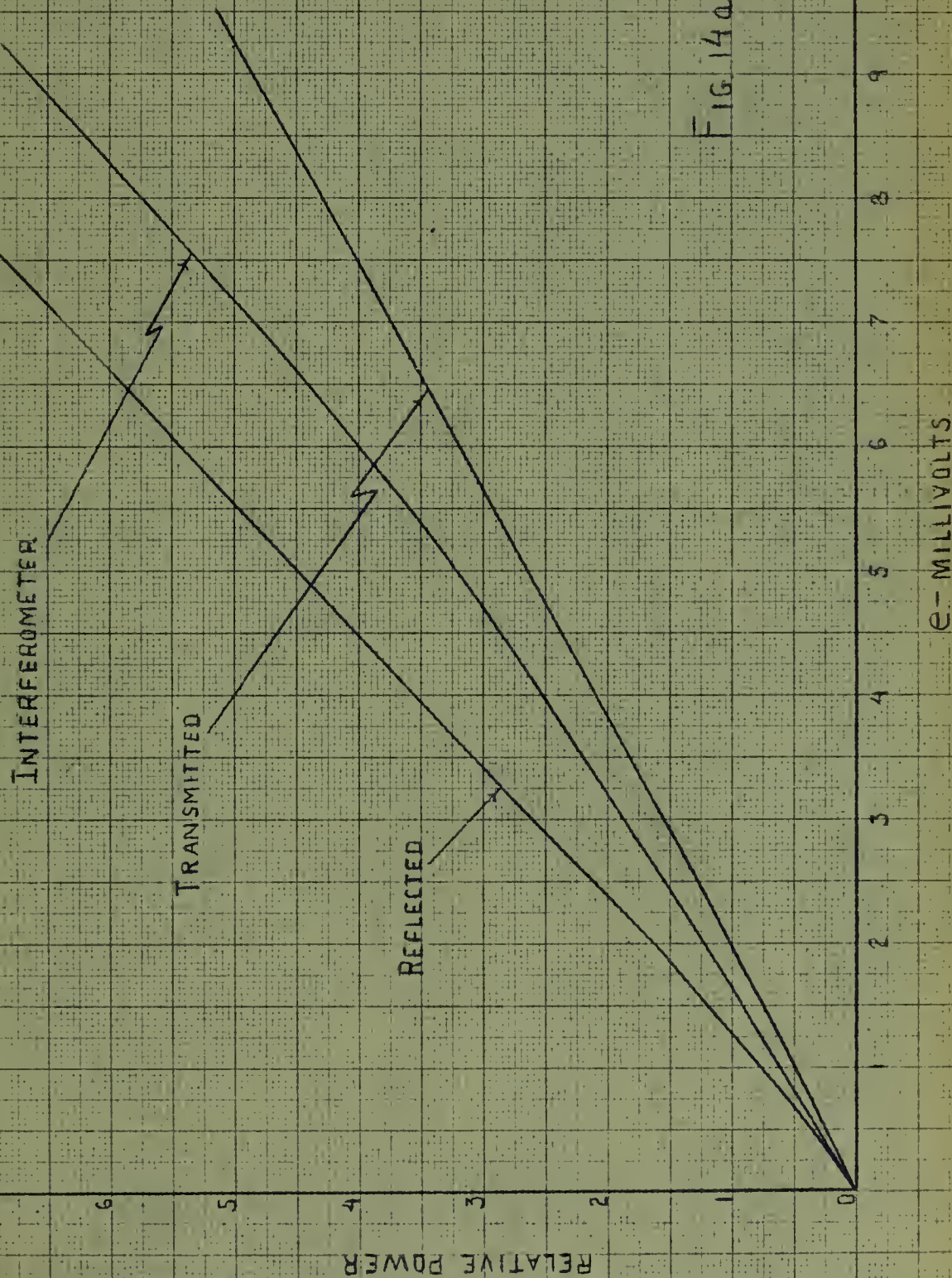
$$\Delta \beta = \frac{\theta}{l} = \frac{.504 \text{ RAD}}{.05 \text{ MET}} = 10.08 \frac{\text{RADIAN}}{\text{METER}}$$

$$\beta = \beta_0 - \Delta \beta = \frac{\omega}{c} - \Delta \beta = 173.22 \frac{\text{RADIAN}}{\text{METER}}$$

$$\alpha = \frac{\ln \frac{P'_{INCIDENT} - P'_{REFL}}{P_{TRANS}}}{2l} = .535$$

CRYSTAL RESPONSE

FIG 14a



CRYSTAL RESPONSE

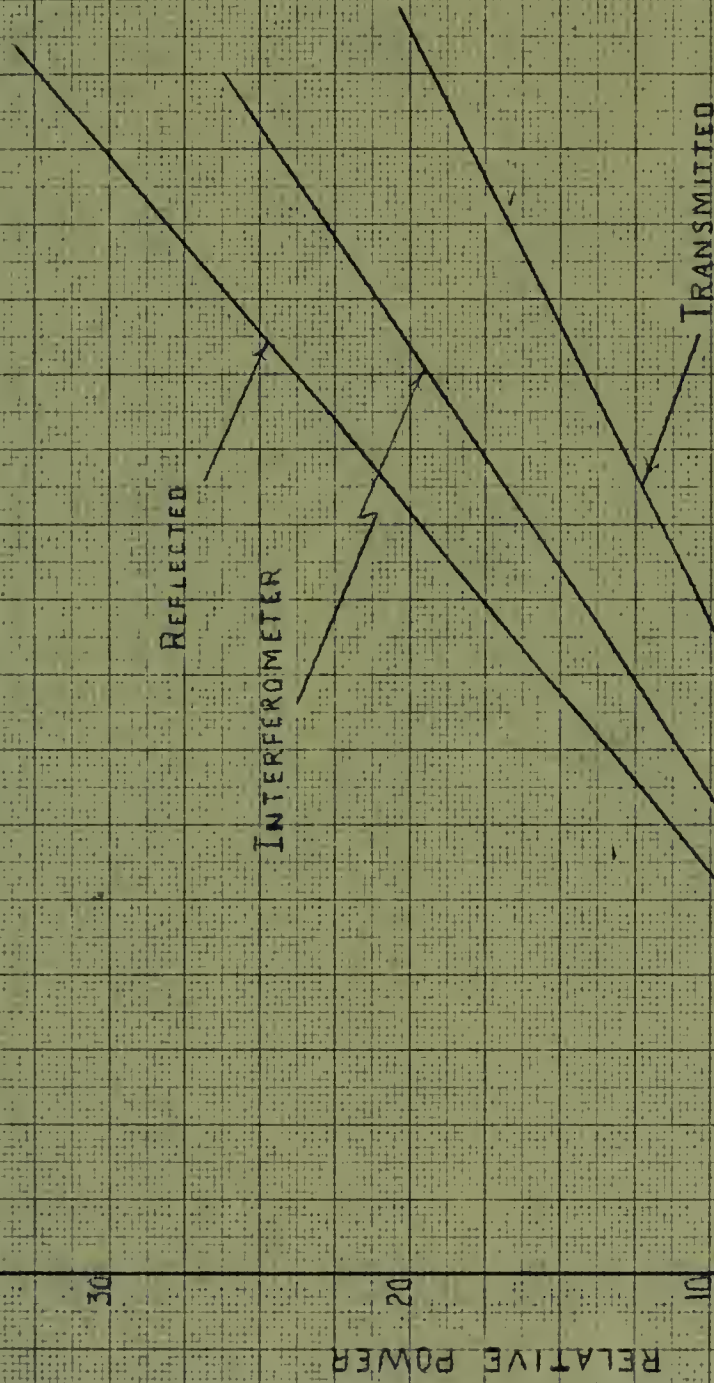


FIG. 14b

Pressure = 11.0 mm Hg									
Time usec	P'int	P'trans	P'refl	Cos θ	ΔB	α	$(\gamma u)^2$	\checkmark	$\frac{1}{N}$ α_r
7400	83.5	12.6	24.4	.422	22.686	17.4	.6098	3.34×10^{10}	.334 3.5×10^{-9}
7900	47.5	22.0	22.2	.793	13.262	13.7	1.014		.519
8400	28.5	39.1	15.6	.885	9.77	9.91	.91		.7082
8900	18.1	59.5	13.2	.917	8.20	5.12	.3673		.856
Pressure = 9.45 mm Hg									
7900	94.5	6.31	20.9	.234	26.6	2.52	.663	2.33×10^{10}	.3045 5.8×10^{-9}
8400	46.4	27.3	19.6	.775	13.76	1.08	.543		.5927
8650	37	40.6	17.3	.810	12.55	.715	.274		.6644
8900	25.2	53.0	9.95	.878	10.08	.535	.261		.8123
9150	16.6	67.2	4.5	.915	8.35	.35	.166		.9824
9400	11.1	81.7	1.50	.942	6.92	.191	.072		1.174
Pressure = 6.23 mm Hg									
9400	59.5	25.5	9.35	.651	16.96	11.2	.3653	$.649 \times 10^{10}$.557 3×10^{-9}
9650	50.0	53.0	5.98	.705	15.8	5.71	11.79		.615
9900	40.5	66.5	4.30	.775	13.72	3.65	.0651		.708
10150	33.3	76.5	2.62	.816	12.3	2.42	.0359		.785
10400	26.2	86.3	1.31	.860	10.8	1.31	.0137		.889

Pressure = 1.21 mm Hg

Time usec	P'int	P'trans	P'refl	Cos θ	ΔB	\propto	$(\frac{dV}{dt})^2$	\checkmark	$\frac{1}{N}$	$\propto r$
2570	52.4	65.0	15.9	.703	15.8	4.12	.075	$.374 \times 10^{10}$.616	3.07×10^{-8}
2620	36.7	75.2	11.4	.798	12.9	2.54	.009		.754	
2670	30.0	82.5	7.5	.837	11.52	1.82	.0055		.843	
2720	19.0	89.8	4.32	.90	9.04	1.31	.005		1.077	

Pressure = .334 mm Hg

950	109.4	37.4	20.4	.212	27.2	7.49	Negl.	$.049 \times 10^{10}$.374	1.7×10^{-8}
1000	88.0	60.6	13.9	.417	22.8	3.5			.432	
1050	64.8	78.7	8.7	.641	17.44	1.66			.571	
1100	49.0	89.8	4.6	.742	14.66	.573			.673	
1150	41.0	95.3	2.07	.790	13.18	.26			.726	
1200	32.8	97.6	.752	.834	11.7	.198			.835	

Table II
Luminosity Calculations

Time	I	\sqrt{I}	$\frac{I}{\sqrt{I}}$
6400	30	5.5	.182
6900	23.5	4.85	.206
7400	17.5	4.20	.238
7900	14.0	3.75	.267
8400	10.5	3.25	.307
8900	8.0	2.83	.353
9400	6.5	2.56	.391
9900	5.0	2.24	.447

Values of $(\frac{V}{\omega})^2$ were only approximate because it was impossible to choose the exact reflected reference level. Consequently, it was necessary to use an arbitrarily chosen reference level. The reference value chosen was the total reflection level (i.e. shorting the transmitting horn). Since the percentage of error due to using this level was less for low values of reflected signal, values for $(\frac{V}{\omega})^2$ were averaged for these low values and used as representative values throughout the decay period [23]. Hence:

$$\left(\frac{V}{\omega}\right)_{AVE}^2 = .1789$$

$$V = \omega \sqrt{.1789} = 2.326 \times 10^{10} \text{ sec}^{-1}$$

$$N = \frac{\omega_p^2 m \epsilon_0}{c^2} = \omega^2 \frac{(\beta_0^2 - \beta^2 + \alpha^2)}{\beta_0^2} \left(1 + \frac{V}{\omega}\right) \frac{m \epsilon_0}{c^2}$$

$$= 1.231 \times 10^{11} \text{ electrons} / \text{cm}^3$$

For pressures of 2 mm or less the approximation for $(\frac{V}{\omega})^2 \ll 1$ could be made and solutions were obtained directly from formulas (15) and (16) in Appendix I.

The recombination coefficient α_r was determined from the slope of the N^{-1} plot of Fig. 8.

$$\begin{aligned}\alpha_r &= \frac{\Delta N^{-1}}{\Delta t} = \frac{(1.174 - .3045) \times 10^{-11}}{9.4 - 7.9 \times 10^{-3}} \\ &= 5.8 \times 10^{-9} \frac{\text{cm}^3}{100\text{-SEC}}\end{aligned}$$

BIBLIOGRAPHY

1. S. G. Homic and R. L. Phillips, Communicating with the Hypersonic Vehicle, *Astronautics*, p36, March 1959.
2. Douglas Aircraft Co., Transmission of EM Waves Through Ionized Air Surrounding Hypersonic Aircraft, Report No. SM 22965, Oct. 1957.
3. Mary F. Romig, Conical Flow Parameters for Air in Dissociation Equilibrium, Convair Scientific Research Lab Note of 14 Jan. 1958.
4. M. A. Heald, Microwave Measurement in Controlled Fusion Research, 1958 IRE National Convention Record Part 9, Medical Electronics and Nuclear Science.
5. C. B. Wharton and D. M. Slager, Microwave Interferometer Measurements for the Determination of Average Electron Density and of Density Profiles, University of California Radiation Laboratory, Livermore UCRL -5244 of 5 June 1958.
6. Romayne F. Whitmer, Microwave Studies of the Electron Loss Process in Gaseous Discharges, *Physical Review*, Vol. 104 No. 3, pp 572-575.
7. K. I. Gringouz, Rocket Measurements of the Electron Concentration in the Ionosphere by Means of an Ultra short Wave Dispersion Interferometer, *Soviet Physics Doklady*, Vol. 3 No. 3, May-June 1958, p620.
8. L. Goldstein, Electrical Discharges in Gases and Modern Electronics, *Advances in Electronics and Electron Physics*, Vol. VII, Academic Press Inc., New York 1955.
9. H. J. Oskam, Microwave Investigation of Disintegrating Gaseous Discharge Plasmas Part I, Phillips Research Laboratories Report, Vol. 13, pp 335-400.
10. H. Margenau, Conduction and Dispersion of Ionized Gases at High Frequencies, *Physical Review*, Vol. 69 Nos. 9 and 10, May 1-15 of 1946.
11. Von Engel, *Ionized Gases*, Oxford at the Clarendon Press, 1956.
12. A. Redfield and R. B. Holt, *Physical Review*, Vol. 82, No. 6, p874.
13. R. A. Johnson and B. T. McClure, *Physical Review*, Vol. 80, No. 3 of 1 November 1950, p376.
14. Skilling, *Fundamentals of Electric Waves*, 2nd edition, John Wiley and Sons, New York, 1945.
15. G. C. Southworth, *Principles and Applications of Waveguide Transmission*, D. Van Nostrand Co., New York.
16. J. Bond. Structure of a Shock Front in Argon, Special Defense Projects Dept. General Electric, 31 August 1956.

BIBLIOGRAPHY

17. H. V. Phelps, O. T. Fundingsland, and Sanford Brown, Microwave Determination of Collision of Slow Electrons in Gases, Physical Review, Vol. 84, No. 3, 1 Nov. 1951.
18. Lyman K. Spitzer, Physics of Fully Ionized Gases, Interscience Publishers Inc., New York, 1956.
19. Manfred A. Biondi, Concerning the Mechanism of Electron-Ion Recombination, Physical Review, Vol. 83, No. 5, 1 Sept. 1951, p1078.
20. E. C. Jordan, Electromagnetic Waves and Radiating Systems, Prentice-Hall, New York, 1950.
21. S. Altshuler and P. Molmud, The Conductivities and Propagation Constants of Ionized Gases, Ramo-Wooldridge Applied Physics Dept. Report.
22. D. L. Fye and H. H. Gunin, Measurement of a Time Varying Complex Propagation Constant in the Microwave Region, NRL Report 4243 of 29 Jan. 1954.
23. H. J. Oskam, Microwave Investigation of Disintegrating Gaseous Discharge Plasmas Part II, Phillips Research Laboratories Report, Vol. 14, pp 401-457.

AG 14 1
SE 19 60
20 AUG 70
20 AUG 70

BINDERY
BINDERY
INTERLIB
Cross 17742
17742

Thesis 41562
A25 Adler
Microwave interfer-
ometer measurements of
electron removal in the
argon afterglow

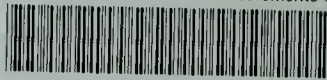
SE 19 60
20 AUG 70
20 AUG 70

BINDERY
INTERLIB
Cross 17742
17742

Thesis 41562
A25 Adler
Microwave interfer-
ometer measurements of
electron removal in the
argon afterglow

thesA25

Microwave interferometer measurements of



3 2768 001 90934 4

DUDLEY KNOX LIBRARY